International Journal of Fatigue 136 (2020) 105577

Contents lists available at ScienceDirect

International Journal of Fatigue

journal homepage: www.elsevier.com/locate/ijfatigue

# Challenging the "$\Delta K_{eff}$ is the driving force for fatigue crack growth" hypothesis

Julián Andrés Ortiz González*, Jaime Tupiassú Pinho de Castro, Marco Antonio Meggiolaro, Giancarlo Luis Gómez Gonzáles, José Luiz de França Freire

*Pontifical Catholic University of Rio de Janeiro, PUC-Rio, R. Marquês de São Vicente 225, Rio de Janeiro 22451-900, Brazil*

ARTICLE INFO

*Keywords:*
Fatigue crack growth
Fatigue crack driving force
Crack-opening load
Effective stress intensity factor range
Crack closure

ABSTRACT

Tests are used to verify the hypothesis "the fatigue crack growth (FCG) driving force is the effective stress intensity factor range $\Delta K_{eff}$". The tests are performed measuring FCG rates in steel and aluminum C(T) and DC(T) specimens under fixed $\{\Delta K, K_{max}\}$ loading conditions and during FCG delays induced by single overloads. Crack-opening loads $P_{op}$ are redundantly measured along the crack path in all tests, using independent near and far field strain-gages, as well as Digital Image Correlation (DIC) techniques. Finally, elastoplastic strain loops within the reverse plastic zone ahead of crack tips are measured using a stereo microscope DIC system.

## 1. Introduction

Paris, Gomez, and Anderson proposed their pioneer approach to describe fatigue crack growth (FCG) showing that FCG rates $da/dN$ correlate well with stress intensity factors (SIF) ranges $\Delta K$ [1]. Based on this idea, Paris and Erdogan proposed their classic parabolic equation $da/dN = A{\cdot}\Delta K^m$, where $\Delta K = K_{max} - K_{min}$ if $K_{min} \geq 0$ [2], which can usually model well phase II FCG under fixed loading conditions. Many similar equations have been proposed to consider relevant FCG effects induced by other parameters, such as peak SIFs $K_{max}$ or load ratios $R = K_{min}/K_{max}$, SIF range FCG thresholds $\Delta K_{th}$, and fracture toughness $K_C$, as reviewed e.g. in [3].

Another approach to model FCG is Elber's $da/dN = f(\Delta K_{eff})$ hypothesis based on plasticity-induced crack closure (PICC) concepts, where $\Delta K_{eff} = K_{max} - K_{op}$ if $K_{op} > K_{min}$, or else $\Delta K_{eff} = \Delta K$ if $K_{op} < K_{min}$, defining $K_{op}$ as the crack-opening SIF. Measuring the compliance of cracked plates along load cycles, Elber identified that fatigue cracks might require tensile opening loads $P_{op} > 0$ to completely open their faces because they grow inside plastic wakes that wrap them [4]. He then assumed that only after the cracks are fully open under loads $P > P_{op}$ they can expose their tips and sustain further fatigue damage ahead of them, supposing in this way that $\Delta K_{eff}$ would be the actual driving force for FCG [5].

Elber's concepts can plausibly rationalize many FCG peculiarities. They can explain e.g. FCG delays and arrests after overloads (OL) assuming the plastic zones $pz_{OL}$ ahead of crack tips hypertrophied by the OL increase $K_{op}$ and thus decrease $\Delta K_{eff}$ in subsequent load cycles while the crack tip is inside $pz_{OL}$. They can explain as well reductions on OL-induced delays after underloads (UL), by the size decrease of previously induced $pz_{OL}$; or else the $R$-dependence of FCG thresholds, assuming $\Delta K_{eff}$ tends to decrease at higher $R$ for a given $\Delta K$ [6–13]. Many works support Elber's hypothesis, as reviewed e.g. by Kemp [14], Skorupa [15–16], and more recently by Pippan and Hohenwarter [17]. Hence, it is not a surprise the $da/dN = f(\Delta K_{eff})$ hypothesis is still popular among many fatigue experts. However, as pointed out by Kemp, many works that support $\Delta K_{eff}$ ideas sustain their conclusions on indirect evidence that do not include proper $K_{op}$ measurements. Therefore, it is not a surprise either that such concepts remain under debate.

Indeed, albeit Elber's postulate can justify many characteristics of the FCG behavior, it cannot explain many others, like FCG delays or arrests after OLs measured under high $R$, when $K_{min} > K_{op}$ [18]; cracks arrested at a given $R$ that restart to grow at a lower $R$ under the same $\Delta K_{eff}$ [19]; or else the $R$-insensitivity of FCG thresholds in inert environments [20]. Such FCG data are incompatible with the $da/dN = f(\Delta K_{eff})$ hypothesis, and based on them the Unified Approach (UA) of Vasudevan et al. questions the actual $\Delta K_{eff}$ role in FCG [21–24]. The UA says that the two FCG driving forces are the SIF range $\Delta K$, which induces cumulative cyclic damage, and the maximum SIF $K_{max}$, which must consider residual stresses due to previous load events while causing peak-dependent damage such as environmentally assisted cracking (EAC) or fracture. The UA says as well that there are two FCG thresholds, one for the SIF range, $\Delta K^*_{th} = \Delta K_{th}(R \rightarrow 1)$, and the other for

* Corresponding author.
*E-mail addresses:* julian@aaa.puc-rio.br (J.A.O. González), jtcastro@puc-rio.br (J.T.P. de Castro), meggi@puc-rio.br (M.A. Meggiolaro), gonzalesglg@aaa.puc-rio.br (G.L.G. Gonzáles), jlfreire@puc-rio.br (J.L.d.F. Freire).

https://doi.org/10.1016/j.ijfatigue.2020.105577
Received 31 August 2019; Received in revised form 16 February 2020; Accepted 3 March 2020
Available online 13 March 2020
0142-1123/ © 2020 Elsevier Ltd. All rights reserved.

the SIF peak, $K^*_{\max th}$. Thus, cracks need to obey two conditions to grow by fatigue, $\Delta K > \Delta K^*_{th}$ and $K_{max} > K^*_{\max th}$. Closure-based crack growth equations ($\Delta K_{eff}$) do not address these thresholds as material properties, while the Unified Approach support that $\{\Delta K, K_{max}\}$ are the true FCG driving forces. According to the UA, these two thresholds are mechanical properties for a given material-environment pair, independent of the geometry, type of loading, and in particular of crack closure. The $R$-independence of FCG thresholds measured in high vacuum mentioned above is a strong evidence to support their last claim, since vacuum suppresses $K_{max}$-dependent EAC effects, but not the plasticity effects that induce crack closure.

The following sections briefly review some arguments that question the use of $\Delta K_{eff}$ in fatigue analyses, and present the methods used to measure $K_{op}$. After studying the various experimental techniques adopted in this work, the comprehensive data set obtained using them is described and analyzed. Finally, since this is not a review paper, see e.g. [18–27] for a list of other fatigue data that cannot be explained by PICC arguments.

## 2. Some $\Delta K_{eff}$ issues

Elber experimentally found in the late 1960's that the apparent stiffness of a fatigue-cracked plate varied during a load cycle, as sketched in Fig. 1a. He then concluded that "as a consequence of the permanent tensile plastic deformation left in the wake of the fatigue crack, one should expect partial crack closure after unloading the specimen" [4]. This is a mechanically sound argument, albeit some dislocation experts question the micro-mechanisms that could form a plastic envelope around the crack faces, the indirect cause for closing them under relatively low tensile loads [28].

As mentioned above, the $\Delta K_{eff}$ postulate can reasonably justify many load order effects in FCG [6–12]. Indeed, soon after Elber's work, von Euw et al. verified the FCG delay behavior expected from PICC concepts, including a short acceleration zone just after the OL due to crack tip blunting, which should locally decrease $K_{op}$ [6]. However, caution is needed when analyzing local FCG rate data, because crack length measurements by classic methods based on potential drop techniques, compliance variations, or traveling microscopes usually have uncertainties around 20 μm [29]. This value may be improved by modern Digital Image Correlation (DIC) techniques, but more optimistic estimates are at least doubtful when not supported by reliable metrological procedures (notice that normally they are not). Modern x-ray microtomography 3D techniques may reach resolutions in the sub-μm range and even identify discrete closed spots along the crack face [30,31], but cracks cannot be treated as simple planar discontinuities inside an isotropic medium at such a resolution level. In any way, arguments based on instantaneous FCG rate data are questionable when not supported by proper calibration.

Such precautions are needed because there are equally reasonable arguments that question the real importance of $\Delta K_{eff}$. Some of them are mentioned in the following, but conflicting data on just one topic can exemplify how controversial this subject can be: plastic zone sizes depend on the dominant stress state around the crack tip, thus on the cracked piece thickness $t$. So, $K_{op}$, $\Delta K_{eff}$, and FCG rates $da/dN$, which depend on $pz$ sizes, should also depend on $t$ if they were really controlled by $\Delta K_{eff}$. However, this thickness-dependence is not always observed in practice. There are data indicating relevant thickness effects on FCG rates [32], and equally respectful data showing this effect is negligible [33]. Radical opinions like "FCG rates are always controlled by $\Delta K_{eff}$" (instead of by $\Delta K$ and $K_{max}$, e.g.) can be seriously questioned with such simple data. In fact, standard FCG measurement procedures are not thickness-dependent: ASTM E647 says thickness effects may be important and recommends (but does not require) that $da/dN$ rates should be measured in specimens as thick as the component the data is intended for, implicitly recognizing thickness effects may be irrelevant.

Anyway, the direct cause for Plastic Induced Crack Closure ($P_{op} > 0$) is the residual stress state induced by the wedge formed by the primarily tensile plastic envelope that surrounds fatigue crack faces on the elastic unbroken ligaments ahead of crack tips, since they would tend to remain undeformed when unloaded. Since only large and strong enough elastic ligaments can induce crack-size independent opening loads, $P_{op}$ induced by smaller ligaments should be crack-size dependent. Therefore, under the same $\{\Delta K, K_{max}\}$ loading conditions, FCG could not be driven by the same $\Delta K_{eff}$ that would drive smaller cracks in such cases. This sound argument motivates the straightforward tests proposed here to verify the universal validity of the $\Delta K_{eff}$ hypothesis, a question that has most important practical consequences, since it addresses the validity of the similitude principle in FCG.

Nevertheless, FCG models based on $\Delta K_{eff}$ concepts are still much used in practice without even considering such a questioning. Indeed, strip-yield models based on PICC are widely used to model FCG under constant and variable amplitude loads (VAL) [9–12], since originally implemented in NASA's NASGRO code [34]. Such models use Forman-Newman's FCG rule assuming $\Delta K_{eff}$ is the FCG driving force. However, since $\Delta K_{eff}$ can only be estimated (unlike $\Delta K$, which can be calculated), it is important to point out two characteristics of this approach that raise some important questions, discussed next.

First, Forman-Newman's rule assumes $da/dN = f(\Delta K_{eff})$ and uses four data fitting parameters $A$, $m$, $p$, $q$, and a transversal constraint factor $\alpha$, frequently used as a fifth adjustable parameter when the other four cannot properly fit a given data set in practice, see Eqs. (1) and (2). This is because their estimate for the opening SIF $K_{op}$, and thus for the effective range $\Delta K_{eff}$, depends on $\alpha$, the ratio between the nominal stress and the Tresca or Mises stress induced by the 3D linear elastic (LE) stress field ahead of the crack tip. Thus, it should vary from $\alpha = 1$ under pure plane stress ($pl$-$\sigma$) to $\alpha = 1/(1 - 2\nu)$ under plane strain ($pl$-$\varepsilon$) dominant conditions, where $\nu$ is Poisson's ratio. Hence, $\alpha$ should depend on the cracked component thickness, and in metallic alloys under $pl$-$\varepsilon$ it

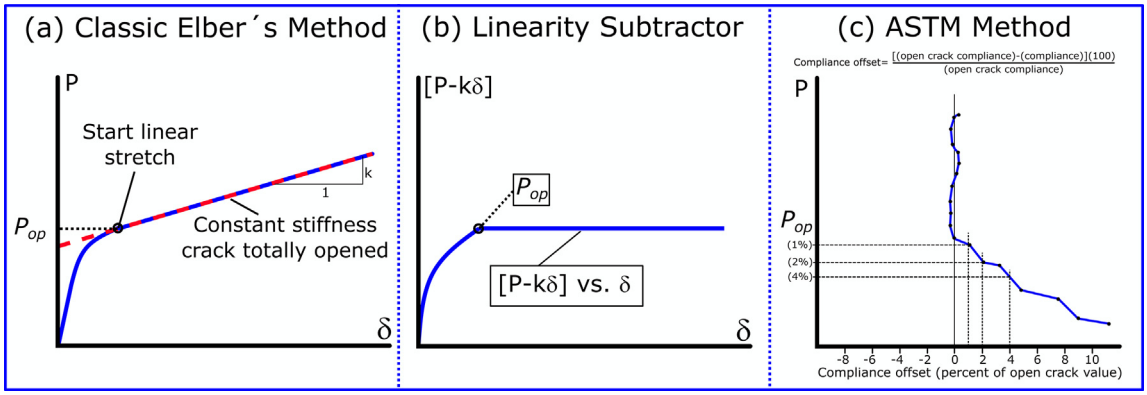


**Fig. 1.** Methods used to measure the crack-opening load $P_{op}$: (a) the classic Elber's method, (b) the linearity subtractor technique, and (c) the ASTM method.

should vary between $2 \leq \alpha_{pl\text{-}\varepsilon} \leq 3$, which have $1/4 \leq \nu \leq 1/3$. However, despite the clear physical meaning of $\alpha$ and its intrinsic geometry and load dependence, in many practical applications it is assumed to be a material constant. For instance, under *pl-ε* conditions, NASGRO recommends $\alpha = 1.5$ for Al 2xxx alloys, $\alpha = 1.9$ for Al 7xxx alloys, $\alpha = 2.0$ for beryllium bronze alloys, and $\alpha = 2.5$ for steels, Ti, and Ni alloys [3,35–36]. Moreover, this FCG rule is indirectly dependent on the load level $\sigma$, where $\sigma$ is the nominal stress and $S_{FL} = (S_Y + S_U)/2$ is the flow strength, defined as the mean of the yielding $S_Y$ and ultimate $S_U$ tensile strengths.

$$\frac{da}{dN} = A\cdot(\Delta K_{eff})^m \frac{(1 - \Delta K_{th}/\Delta K)^p}{(1 - K_{\max}/K_C)^q} \tag{1}$$

$$\begin{cases} \frac{K_{op}}{K_{\max}} = \begin{cases} \max[R,\ (A_0 + A_1 R + A_2 R^2 + A_3 R^3)],\ R \geqslant 0 \\ A_0 + A_1 R,\ -2 \leqslant R < 0 \end{cases} \\ A_0 = (0.825 - 0.34\alpha + 0.05\alpha^2)\cdot[\cos(\pi\sigma_{\max}/2S_{FL})]^{1/\alpha} \\ A_1 = (0.415 - 0.071\alpha)\cdot\sigma_{\max}/S_{FL} \\ A_2 = 1 - A_0 - A_1 - A_3 \\ A_3 = 2A_0 + A_1 - 1 \end{cases} \tag{2}$$

The second characteristic of the Forman-Newman approach is that these opening SIFs $K_{op}$ and $\Delta K_{eff}$ values are based on 1D strip-yield mechanics estimates for large center-cracked plates, which are questionable when applied for other cracked components, especially under VAL. There are corrections for many of them [36], but not a universal one yet. These points are explored in [37–39], which propose Critical Damage Models (CDMs) based on the very same strip-yield mechanics used on NASGRO-like codes, but assuming FCG is caused by damage accumulation ahead of crack tips, recognizing the existence of closure but not the zero-damage hypothesis on a partially closed crack.

Such questions clearly indicate that good $P_{op}$ measurements are essential to verify the $\Delta K_{eff}$ hypothesis. Rational arguments alone are not enough to check it. Indirect evidence such as good FCG data fitting is not a proof of its validity either, as discussed by Kujawski [26]. That is why $P_{op}$ measurement methods are briefly reviewed in the following.

Elber defined $P_{op}$ as the load that fully opens a fatigue crack, exposing its tip. He used a stiffness curve $P$–$\delta$ to measure it, where $P$ is the load applied on the cracked specimen and $\delta$ is the displacement of its application point [4], or a parameter proportional to it. This can be done e.g. by tracing a tangential line starting at $P_{max}$ (P–$\delta$ curves have a linear part after the crack is fully opened if the ligament remains primarily LE) and identifying $P_{op}$ at the point where the tangent line and the stiffness curve separate, see Fig. 1a. To facilitate the identification of $P_{op}$, Paris and Hermann proposed to use the slope of that tangent ($\kappa$ in Fig. 1a) to plot a new [$P$ - $\kappa\delta$]vs. $\delta$ curve, which allows $P_{op}$ to be more easily located at the point where its horizontal portion starts, see Fig. 1b [40]. ASTM E647 FCG standard accepts a Compliance Offset Method that uses this same idea to measure $P_{op}$, as sketched in Fig. 1c, recommending a 2% offset to measure $P_{op}$, but also accepting 1% and 4%, a questionable operational criterion in view of Elber's $P_{op}$ definition.

On the other hand, after finding some problems in the $\Delta K_{eff}$ hypothesis, Kujawski specified $P_{op}$ using two tangents to the stiffness curve, one at the apparent end $P_1$ of its lower straight part and the other at the apparent start $P_3$ of its upper straight part. The intersection of these two tangents define $P_2$, and $P_{op}$ is chosen as the load near $P_2$ that better collapses the FCG data for different *R-ratios* in a single $dN$–$\Delta K_{eff}$ curve, a controversial procedure that uses $P_{op}$ as an adjustable instead of a measurable parameter. Nevertheless, Kujawski concluded that the collapsing of FCG data does not necessarily prove that $\Delta K_{eff}$ is indeed the crack driving force [26].

Elber's $\Delta K_{eff}$ hypothesis assumes that only loads $P > P_{op}$ can further damage the material ahead of fatigue crack tips during any load cycle, supposing the material ahead of them remains totally shielded from elastoplastic (EP) strains, the main cause for fatigue damage, while their tips are closed. Fig. 2a schematizes EP stress/strain loops inside cyclic plastic zones ahead of crack tips without crack closure, whereas Fig. 2b shows the expected loops with the assumed closure effect. The behavior shown in Fig. 2b is idealized from Elber's hypothesis, since assuming no fatigue damage below $P_{op}$ would imply in no strain increments in those loops for loads $P < P_{op}$.

Based on it, Ferreira et al. [38] mention that even the loops presented by Elber himself [5] could be used to question his own hypothesis "the material ahead of the crack does not suffer any fatigue damage under loads $P < P_{op}$". Many other representative experiments that cannot be properly modeled by $\Delta K_{eff}$ concepts are described elsewhere [38,41–45]. Hence, there is no need to repeat them here, albeit they are important to justify the need for the tests presented in this work.

The next section describes the experimental setup used in this work to measure the set of data needed to verify whether $\Delta K_{eff}$ is indeed the only or even the main driving force for FCG.

## 3. Experimental setup

As discussed above, careful measurements of opening loads $P_{op}$ along fatigue crack paths are a necessary condition to unambiguously verify $\Delta K_{eff}$ concepts. This is the main reason for choosing to grow fatigue cracks in standard Disk-Shaped Compact DC(T) and Compact C(T) specimens under fixed or quasi-fixed {$\Delta K$, $K_{max}$} conditions according to ASTM E647 procedures. Crack lengths $a$ are measured by the traditional compliance technique, using a strain gage bonded on the back face of the specimens and a data acquisition system. Moreover, such analog crack length measurements are verified frequently by optical means as the cracks grow during the FCG tests, using either a traveling microscope, a Digital Image Correlation (DIC) system, or both. All tests are performed in a properly calibrated 100kN Instron computer-controlled servo-hydraulic fatigue-testing machine. $\Delta K$ and $K_{max}$ values are calculated in real time using the standard ASTM E399 SIF equations.

In the first stage of this test program, the loading conditions {$\Delta K$, $K_{max}$} are kept quasi-constant by repeatedly decreasing the applied loads after small crack growth increments, typically $\Delta a \cong 0.1$ mm or less, following standard ASTM E647 procedures. In subsequent tests, the loads are continuously adjusted and controlled in real time by a specially developed LabView program to maintain fixed {$\Delta K$, $K_{max}$} conditions. This program calculates SIFs using the measured crack length and load cell signals, using them as the control signal to adjust in real time the loads applied on the specimen. The program continuously plots $a$ vs. FCG rate and $\Delta K$ charts as well.

The crack-opening load $P_{op}$ is redundantly measured both by Elber's tangent and by linearity-subtractor procedures, see Fig. 1, using a far-field signal from a strain gage bonded on the back-face of the specimen, while the near-field signal is obtained from a strip with 10 gages bonded ahead of the crack tip. $P_{op}$ values measured by the near and the far-field gages showed no major discrepancy, meaning that essentially the same $P_{op}$ value was obtained from both in all tests.

Additionally, a Digital Image Correlation (DIC) system from Correlated Solutions is used to obtain two other types of redundant $P_{op}$ measurements, as well as to verify the crack length [47]. This system allows accurate measurements of displacement/strain fields on the specimen surface [48]. It includes two 5-MP Point Grey GRAS-50S5M CCD monochromatic cameras with Tamron SP AF180mm F/3.5 lenses, a double fiber-optic light source, calibration grids, a data acquisition system, and the software package VIC-3D. The digital cameras are mounted on a tripod in front of the specimen in a stereo configuration, to allow the measurement of the entire 3D displacement field, i.e., of its $x$, $y$, and $z$ components, see Fig. 3.

The images collected during the fatigue tests are processed by the VIC-3D software using a subset window size of 35 pixels, step size of 8 pixels, strain window size of 15, and cross correlation function of the normalized sum of squared differences. Since the load is applied in the vertical direction, the $v$-displacement and the corresponding $\varepsilon_y$ strain

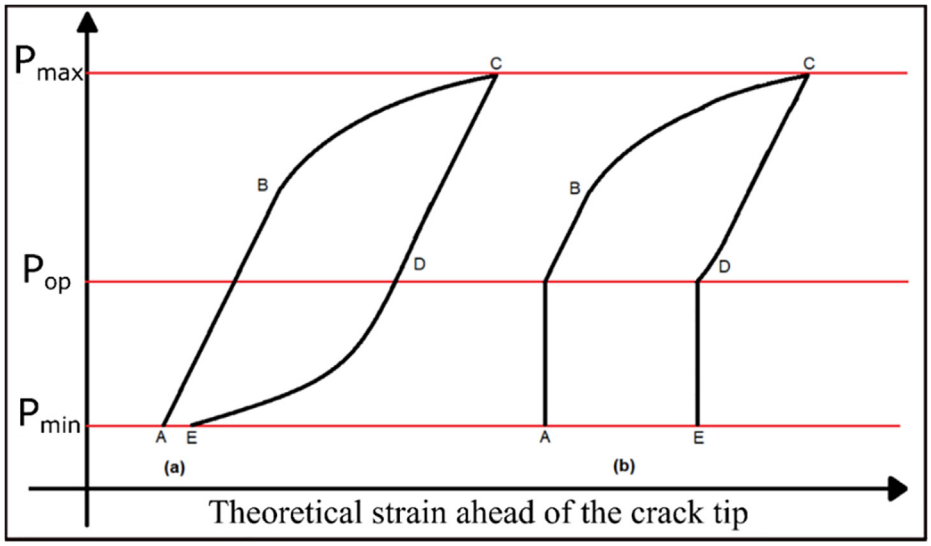


**Fig. 2.** Schematic load vs. strain loops inside the cyclic plastic zone $pz_c$ ahead of a fatigue crack tip, (a) without and (b) with crack closure effects [37].

map are used to identify the crack-opening load. A pair of symmetrical points is located along the crack faces at *2* mm behind the crack tip to obtain near crack-opening displacement (COD) measurements from the *v*-displacement field. Furthermore, the strain history in the *y*-direction is collected from a point located *1* mm ahead of the crack tip. For further details on the experimental procedures, see [46,48].

First, FCG tests are performed on ASTM E399 standard Disk-Shaped Compact Tension DC(T) specimens of AISI 1020 steel with two different thicknesses, *2* and *30* mm, to simulate plane stress and plane strain conditions, respectively. All specimens were cut from the same *76* mm diameter bar with yield and ultimate strengths $S_Y = 262$ MPa and $S_U = 457$ MPa. The dimensions and chemical composition of the AISI 1020 steel specimens tested in this work are shown in Fig. 4.

Since these specimens are tested under quasi-constant $\{\Delta K = 20$ MPa$\sqrt{m}, R = 0.1\}$ conditions, their thicknesses $t$ were chosen to maintain nominally plane stress conditions in the thin $t = 2$ mm specimens (making the plastic zone that always follows the fatigue crack tips $pz > t$), and plane strain in the thick $t = 30$ mm ones. This choice assumes ASTM E399 plane strain requirements can be used in FCG as well, i.e. if $t > 2.5\cdot(K_{max}/S_Y)^2$. Indeed, using Irwin's estimate for the $pz$ ahead of the crack tip, assuming this traditional 2D view is appropriate to define a plane stress state in FCG, then $t = 2$ mm $pz_{max} = (1/\pi)\cdot(K_{max}/S_Y)^2 = (1/\pi)\cdot[20/(0.9\cdot262)]^2 = 2.29$ mm $> t$. On the other hand, specimens with $t = 30$ mm have $t > 2.5\cdot(K_{max}/S_Y)^2 = 2.5\cdot[20/(0.9\cdot262)]^2 = 17.99$ mm, so their cracks supposedly grow under nominally plane strain conditions.

Similar FCG tests are then replicated in a 6351-T6 Al alloy, whose compact microstructure is FCC, instead of the non-compact BCC microstructure of the 1020 steel. Moreover, to verify improbable but possible specimen type effects, both standard DC(T) and Compact Tension C(T) specimens, with two different thicknesses $t = 2$ mm and $t = 30$ mm, are tested to simulate *pl-σ* and *pl-ε* FCG conditions, respectively. All specimens were cut from the same *76* mm diameter wrought round bar with yield and ultimate strengths $S_Y = 170$ MPa and $S_U = 290$ MPa. Specimen dimensions and the chemical composition of this 6351-T6 Al alloy are shown in Fig. 5.

The Al specimens are loaded under quasi-constant $\{\Delta K = 15$ MPa$\sqrt{m}, R = 0.1\}$ conditions. Thus, for the thin specimens $t = 2$ mm $< pz_{max} = (1/\pi)\cdot(K_{max}/S_Y)^2 = (1/\pi)\cdot[15/(0.9\cdot170)]^2 = 3.05$ mm, whereas for the thick ones $2.5\cdot(K_{max}/S_Y)^2 = 2.5\cdot[15/(0.9\cdot170)]^2 = 24$ mm $< t = 30$ mm. These thicknesses confirm the *pl-σ* and *pl-ε* conditions assumed above (using the same ASTM E3399 criterion applied to the steel specimens, assuming it remains valid for FCG).

In addition, the effect of single overloads is investigated. Such tests are made under *pl-σ* and *pl-ε* conditions, to observe the $\Delta K_{eff}$ behavior before and after the OLs, in the delay region. First, the crack is grown far from the notch influence zone, to achieve a stable FCG rate. Then, a single OL $K_{OL} = 2\cdot K_{max}$ is applied and the quasi-constant $\{\Delta K, K_{max}\}$ loads are retaken.

Finally, a 3D stereo microscope DIC system is used to measure the strain fields ahead of crack tips with higher resolution. It has also been provided by Correlated Solutions, and contains a stereo microscope Olympus SZX16 equipped with two 5.0 megapixel CCD cameras mounted on a 3-axis motorized stage for fine position control. This system uses a patented distortion correction software that computes the non-parametric distortion fields of the microscope, to eliminate shape and strain bias from the measurements, while overcoming the problems

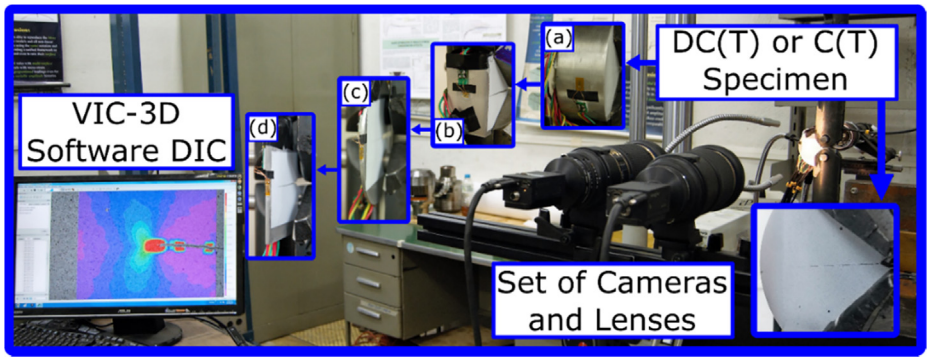


**Fig. 3.** Experimental setup used to measure displacement/strain fields on the specimen surface with the DIC system, showing a strain field resulting from it on the lower left. Four different specimens are used in this work: (a) plane strain DC(T), (b) plane strain C(T), (c) plane stress DC(T), and (d) plane stress C(T). Notice the back face strain gages bonded on them.

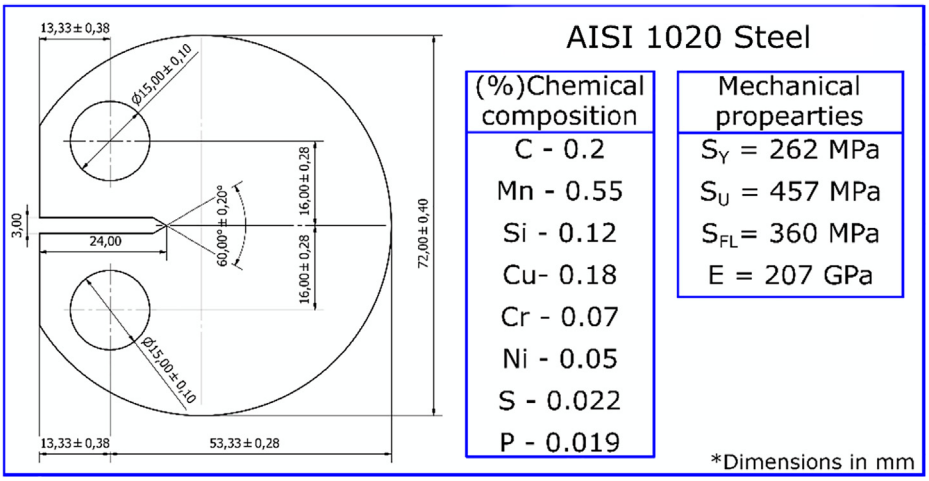


**Fig. 4.** Dimensions of DC(T) specimens and chemical composition of the tested AISI 1020 steel.

associated with 3D measurements under high magnification. The stereo microscope is configured to analyze an area of about $3 \times 3.5$ mm on the specimen surface. The calibration of the cameras is performed using a standard calibration grid of $15 \times 15$ dots with dots spaced by 110 μm. The smaller speckle pattern on the specimen surface, required to achieve a high resolution in DIC measurements, is created by carefully spraying toner powder over a white paint background. The speckle pattern and experimental setup used for near-crack tip DIC analyses are illustrated in Fig. 6 [48].

In the tests with the stereo microscope DIC system, the strain field around the crack tip is also measured with the conventional DIC system described above, but placed on the opposite surface of the specimen. Like in all other tests, this system is used to make redundant $P_{op}$ measurements, adopting the procedures already described. Due to that, it was not possible to bond strain gage strips in front of the crack tip in these tests. However, a strain gage was bonded on the back face of the specimens to measure the crack length and the corresponding $P_{op}$. To simplify, Table 1 shows a summary of the characteristics of each test, indicating the figures where their results are presented.

## 4. Experimental results

The first tests with both DIC and strain gage compliance measurements in 1020 steel specimens maintain quasi-constant $\{\Delta K = 20$ MPa√m, $R = 0.1\}$ load conditions with manual control as the cracks grow, to duplicate and verify the results obtained in previous works [41]. Figs. 7 and 8 depict the evolution of the FCG rates and of the crack-opening ratios $K_{op}/K_{max}$ measured along the crack path in *pl-σ* and *pl-ε*, respectively. The crack size in these figures is quantified by $a/w$, the ratio between the crack length $a$ and the original (uncracked) ligament size $w$, measured from the load line. Opening load measurements (quantified by $K_{op}/K_{max}$) use a specially developed piece of software written in MATLAB to numerically implement the straight-line fitting and the linearity-subtractor techniques described in [29], applying them to the redundantly measured $P$–$\varepsilon$ near and far-field signals.

Figs. 7 and 8 show that the measured FCG rates in the four specimens remain essentially constant (i.e., within the noise level associated with discrete step-wise load adjustments) during these tests. Moreover, such FCG rates do not depend on the specimen thicknesses, even though in the thinner ones the cracks grow under nominally *pl-σ* conditions, whereas in the thicker ones they grow under *pl-ε*, according to traditionally accepted criteria. Hence, these experiments confirm the classic ASTM view that FCG rate curves $da/dN$–$\Delta K$ measured under fixed *R-ratios* can properly characterize and quantify the FCG behavior of structural materials, at least when applied to the tested steel.

They also confirm the idea that $\{\Delta K, K_{max}\}$ are the FCG driving forces in them, or at least cannot be used to question it. Hence, such tests reassure the basic principle that the SIF range $\Delta K$ can be used as a similitude parameter in FCG predictions. On the other hand, these data cannot be explained by the alternative view that FCG is driven by $\Delta K_{eff}$. Indeed, those simple tests, which follow just straightforward and well-stablished procedures, clearly show that the crack-opening ratio $K_{op}/$

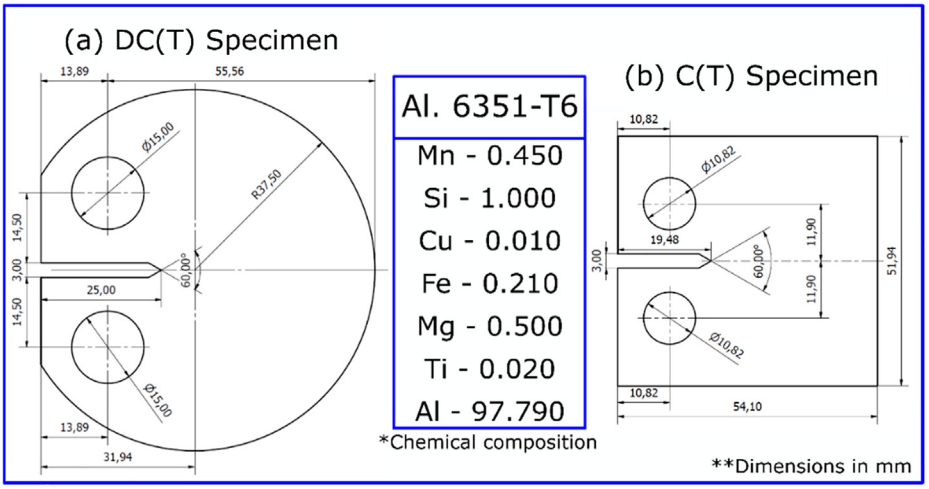


**Fig. 5.** Dimensions of the (a) DC(T) and (b) C(T) specimens and chemical composition of the tested 6351-T6 Al alloy.

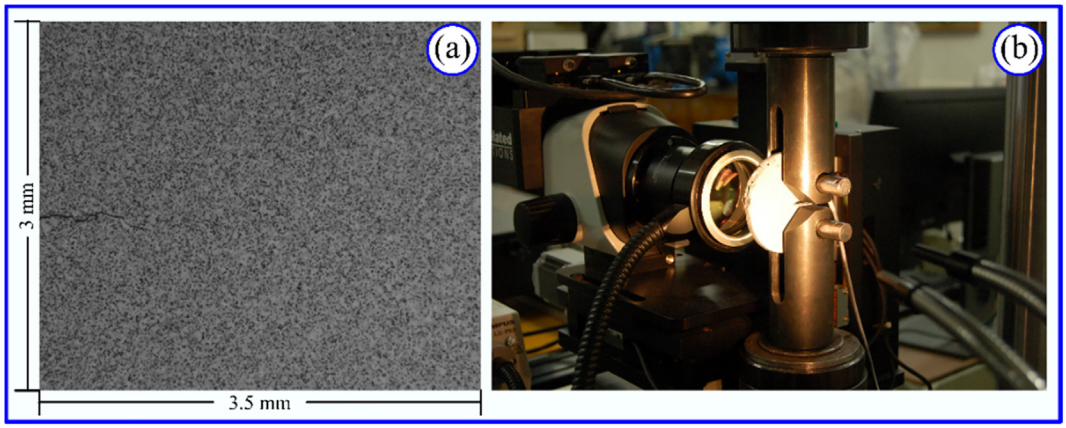


**Fig. 6.** (a) Toner powder fine pattern and (b) experimental setup used for the experiments with the stereo microscope DIC system.

**Table 1**
Summary of the characteristics of each test.

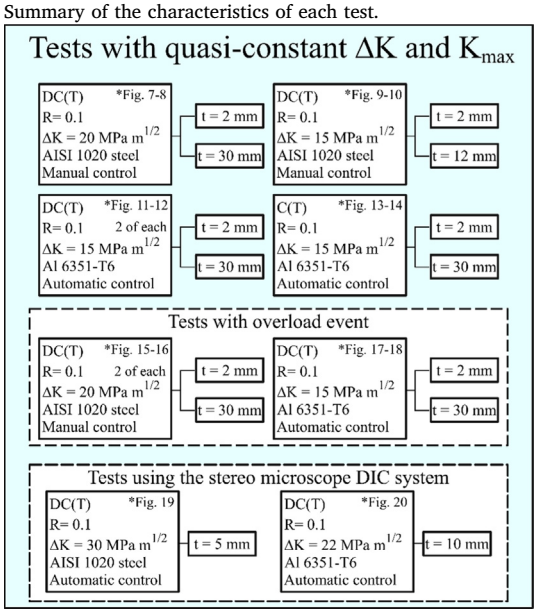


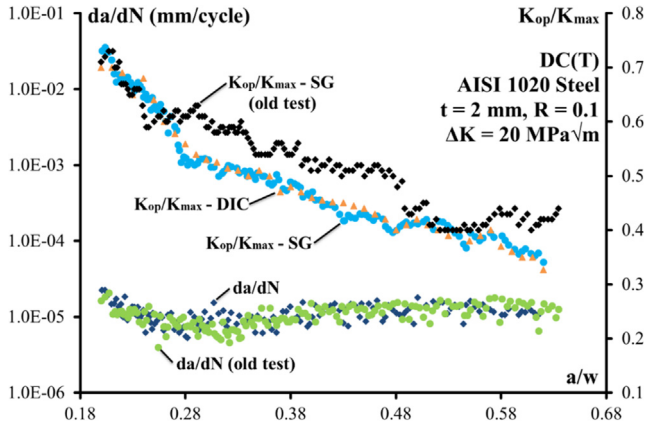


**Fig. 7.** FCG rates $da/dN$ and crack-opening ratios $K_{op}/K_{max}$ continuously measured under quasi-constant amplitude loading conditions (namely $\{\Delta K = 20$ MPa√m, $R = 0.1\}$) in thin DC(T) specimens ($t = 2$ mm) of 1020 steel.

$K_{max}$ steadily decreases in both the thin and the thick specimens as their cracks increase in size, decreasing the (predominantly elastic) residual ligament that tends to close them. Since quasi-constant amplitude loading $\{\Delta K, K_{max}\}$ conditions were maintained during those tests,

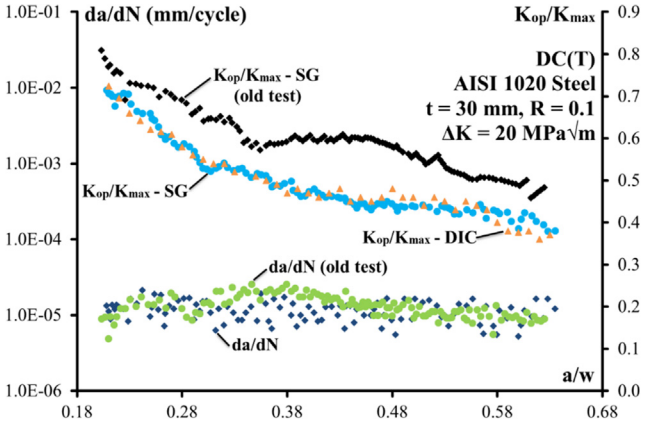


**Fig. 8.** FCG rates $da/dN$ and crack-opening ratios $K_{op}/K_{max}$ continuously measured under quasi-constant amplitude loading conditions (namely $\{\Delta K = 20$ MPa√m, $R = 0.1\}$) in thick DC(T) specimens ($t = 30$ mm) of 1020 steel.

there is no doubt that $\Delta K_{eff}$ steadily increased as the cracks grew, because the decrease in $K_{op}/K_{max}$ ratio was well beyond the (relatively small) uncertainty of the measured data. These results are similar to the ones from the previous 1020 steel tests reported in [41].

Notice as well that, despite the very same overall decreasing behavior while the crack grows, the values of the old and new $K_{op}/K_{max}$ measurements depicted in these figures are not as similar as the values of the FCG rates $da/dN$ measured at the same time (Fig. 7 and Fig. 8). Since $\Delta K_{eff}$ is not their FCG driving force, and since $K_{op}$ can be caused by other mechanisms besides PICC (roughness induced closure, e.g.), this result is neither surprising, nor an evidence they may be unreliable. Indeed, the variability in the $\Delta K_{eff}$–$a/w$ measurements without a corresponding variability on the measured $da/dN$ rates just supports the idea that crack closure is not playing a major role in these tests.

To reinforce this claim, two similar 1020 steel DC(T) specimens are tested under smaller quasi-constant $\{\Delta K = 15$ MPa√m, $R = 0.1\}$ loadings, see Figs. 9 and 10, using the same redundant techniques to measure $P_{op}$. Under this new load, if follows that $K_{max} = \Delta K/(1 - R) = 16.66$ MPa√m and thus Irwin's plastic zone is $pz_{max} = (1/\pi)\cdot(16.66/262)^2 = 1.3$ mm. Hence, the thin $t = 2$ mm specimen grows its crack under dominant (but maybe not pure) $pl$-$\sigma$ conditions, since $t \cong pz_{max}$. The thick $t = 12$ mm one grows its crack under $pl$-$\varepsilon$, since $2.5\cdot(K_{max}/S_Y)^2 = 2.5\cdot(16.66/262)^2 = 10.11 < t = 12$ mm.

The near and far-field redundant $P_{op}$ measurements based on DIC and on strain gage techniques are once again very similar, so there is no need to separate them in Figs. 9 and 10 either. Notice the significant decrease in the measured $K_{op}/K_{max}$–$a/w$ curve while the curve for the

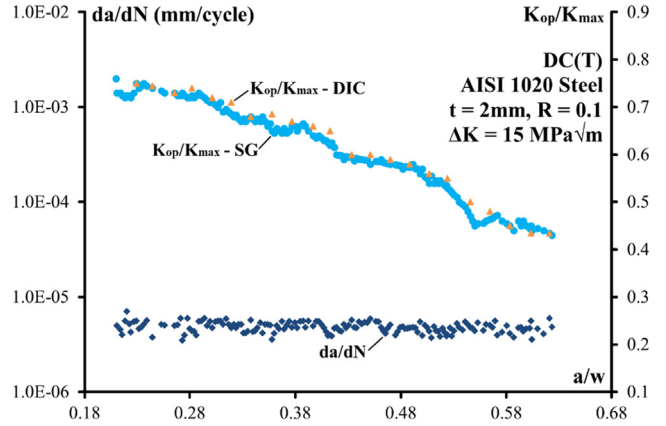


**Fig. 9.** FCG rates $da/dN$ and crack-opening ratios $K_{op}/K_{max}$ continuously and redundantly measured by near and far field DIC and strain gage compliance techniques under quasi-fixed loading conditions $\{\Delta K = 15$ MPa√m, $R = 0.1\}$ in a thin 1020 steel DC(T) specimen, with $t = 2$ mm.

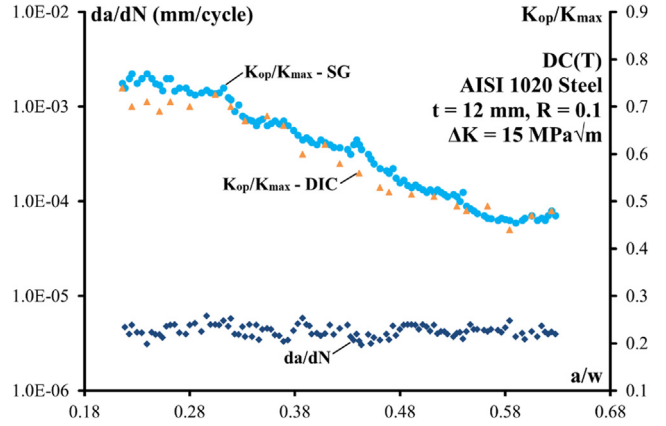


**Fig. 10.** FCG rates $da/dN$ and crack-opening ratios $K_{op}/K_{max}$ continuously and redundantly measured by near and far field DIC and strain gage compliance techniques under quasi-fixed loading conditions $\{\Delta K = 15$ MPa√m, $R = 0.1\}$ in a thick $t = 12$ mm 1020 steel DC(T) specimen.

FCG rate $da/dN$–$a/w$ remains essentially constant (and smaller than in Figs. 7 and 8) during the entire test. Such data has an overall $K_{op}/K_{max}$–$a/w$ decreasing behavior similar to the behavior of the data depicted in Figs. 7 and 8, hence it clearly shows that $\Delta K_{eff}$ is not the controlling FCG driving force in these tests either.

To rule out a possible material-dependent behavior, similar tests on 6351-T6 Al are made under fixed $\{\Delta K = 15$ MPa√m, $R = 0.1\}$ loads, in two thin and two thick DC(T)s, to obtain *pl-σ* and *pl-ε* FCG conditions. Such loads are called *fixed* because a significant improvement on the test procedures is introduced in such tests to decrease even more data dispersion: they are controlled by a closed loop system in real time using the calculated SIF as the control signal, as described before.

As shown in Figs. 11 and 12, the dispersion in $da/dN$ FCG rates indeed decreases significantly, but the very same decreasing trend on $K_{op}/K_{max}$ ratios is observed in these Al tests, confirming that $\Delta K_{eff}$ is not their controlling FCG driving force either. Notice that the $K_{op}/K_{max}$ data measured by the four independent strain gage and DIC-based techniques once again yield quite similar results. Indeed, the decrease in $K_{op}/K_{max}$–$a/w$ curves is as significant as the one obtained for the steel specimens. Moreover, the much less dispersed FCG rates indicate that the real time load adjustment to maintain constant $\{\Delta K, R\}$ conditions is in fact quite efficient. Finally, to avoid any doubts about the property of testing non-standard FCG DC(T) specimens (such specimens are accepted by ASTM E399 but not by the E647 standard, albeit they should be), the same tests are repeated in standard C(T) specimens under the

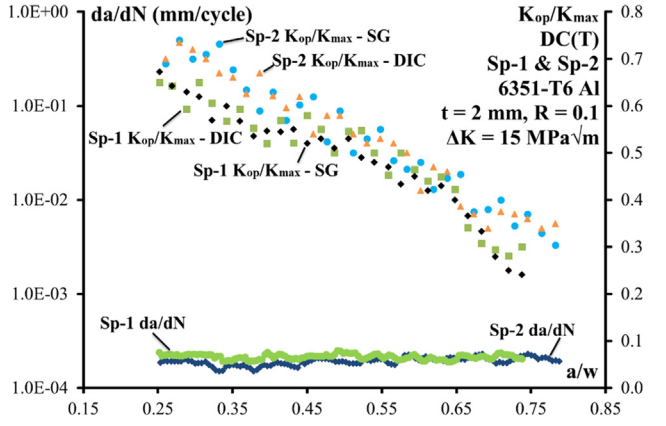


**Fig. 11.** FCG rates $da/dN$ and crack-opening ratios $K_{op}/K_{max}$ continuously and redundantly measured by near and far field DIC and strain gage compliance techniques under quasi-fixed loading conditions $\{\Delta K = 15$ MPa√m, $R = 0.1\}$ in thin 6351-T6 Al DC(T)s, with $t = 2$ mm.

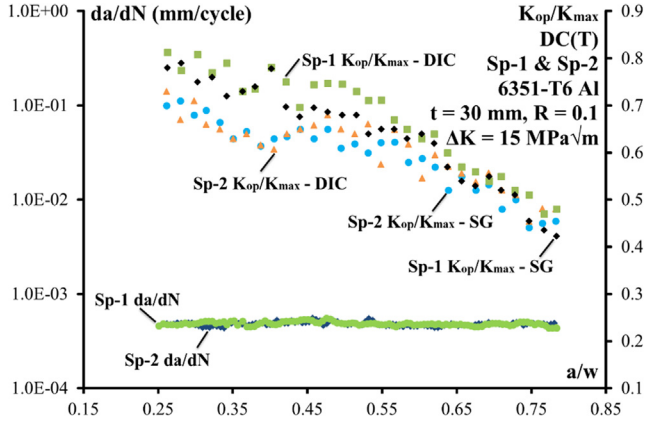


**Fig. 12.** FCG rates $da/dN$ and crack-opening ratios $K_{op}/K_{max}$ continuously and redundantly measured by near and far field DIC and strain gage compliance techniques under quasi-fixed loading conditions $\{\Delta K = 15$ MPa√m, $R = 0.1\}$ in thick 6351-T6 Al DC(T)s, with $t = 30$ mm.

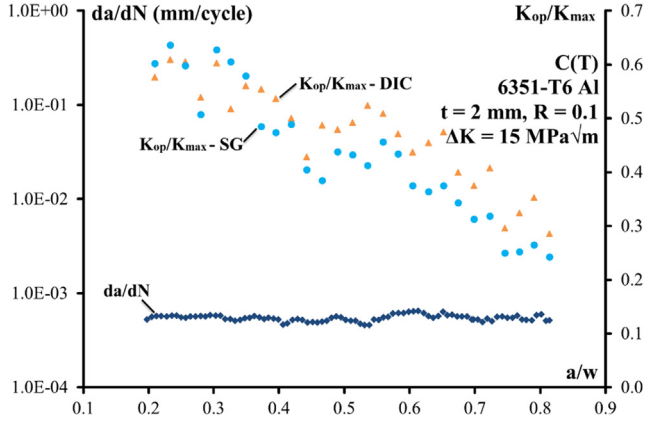


**Fig. 13.** FCG rates $da/dN$ and crack-opening ratios $K_{op}/K_{max}$ continuously and redundantly measured by near and far field DIC and strain gage compliance techniques under quasi-fixed loading conditions $\{\Delta K = 15$ MPa√m, $R = 0.1\}$ in a thin 6351-T6 Al C(T), with $t = 2$ mm.

same constant $\{\Delta K = 15$ MPa√m, $R = 0.1\}$ loading conditions, see Figs. 13 and 14.

The specimen type should not be an issue, because in principle FCG rates could be measured in any specimen whose SIF is known, since

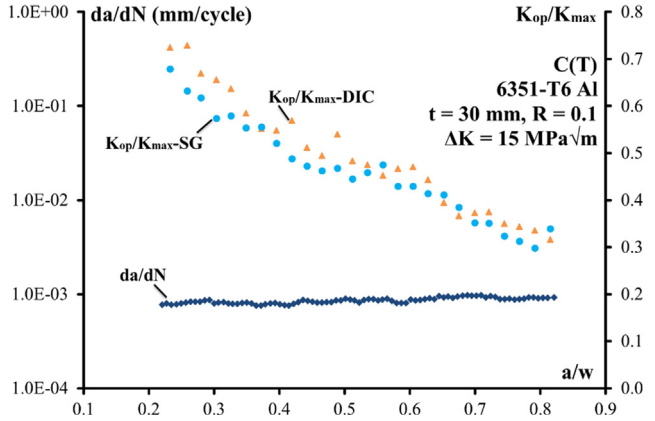


**Fig. 14.** FCG rates *da/dN* and crack-opening ratios $K_{op}/K_{max}$ continuously and redundantly measured by near and far field DIC and strain gage compliance techniques under quasi-fixed loading conditions {$\Delta K = 15$ MPa√m, $R = 0.1$} in a thick 6351-T6 Al C(T), with $t = 30$ mm.

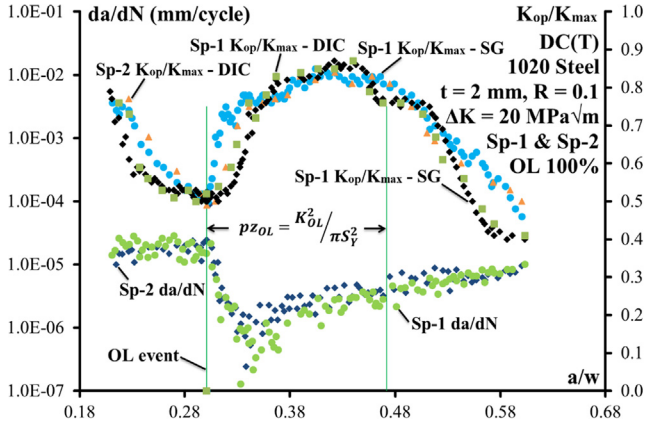


**Fig. 15.** FCG rates *da/dN* and crack-opening ratios $K_{op}/K_{max}$ continuously measured under quasi-constant amplitude loading conditions {$\Delta K = 20$ MPa√m, $R = 0.1$}, before and after a single OL with $K_{OL} = 2{\cdot}K_{max}$, in two thin 1020 steel specimens with $t = 2$ mm.

they are intended to be used in any structural component assuming the SIF-similitude principle. Anyway, the data obtained from C(T) specimens show once again the very same $K_{op}/K_{max}$ decreasing behavior as the crack length increases observed in DC(T)s, while the FCG rate remains practically constant during the entire tests, both in *pl-σ* and in *pl-ε*. Hence, it can be claimed that the experimental data obtained above shows that $\Delta K_{eff}$ is not the controlling FCG driving force in any of them, independent of the studied material, load level, and specimen type.

Notice that, like in the steel tests, the measured $P_{op}$ behavior of the Al alloy is not identical in all tested specimens. This indicates that $K_{op}$ is not a property of the geometry/load pair. Instead, it can vary in nominally identical specimens submitted to equal loading conditions not only with the relative crack size *a/w*, but it can also depend on local details along the crack path, probably because it is or can be affected by non-PICC mechanisms.

Notice as well that the FCG rates *da/dN* measured in the various Al specimens, although far less dispersed along the crack paths due to the automated load control, show a slightly higher variation among specimens than the rates measured in the various steel specimens. In particular, the rates measured in the C(T) specimens are a little higher than the rates measured in the DC(T)s. However, no conclusions can be drawn from this observation, because the presented data is not extensive enough to do so. Anyway, since this topic is beyond the scope of this paper, it is not pursued here. Finally, notice that all tests described above support the idea that *da/dN*–$\Delta K$ curves (instead of da/dN–$\Delta K_{eff}$ curves) can be used to describe the material FCG resistance, suggesting that codes that use them to simulate FCG lives can be reliably used in practical applications.

### 4.1. Single overload tests

Single overload tests are now performed on thin $t = 2$ mm and thick $t = 30$ mm DC(T)s 1020 steel specimens, keeping {$\Delta K = 20$ MPa√m, $R = 0.1$} almost constant both before and after the OL through manual control. $P_{op}$ is measured by the same near and far field procedures explained before. The cracks grow under almost constant {$\Delta K$, $R$} load conditions until they reach a size $a \cong 5$ mm, when a single *100%* OL on $K_{max}$ ($K_{OL} = 44.44$ MPa√m) is applied. Next, the almost constant {$\Delta K$, $R$} loading conditions are reapplied to continue propagating the crack. Fig. 15 shows the FCG rates *da/dN* and $K_{op}/K_{max}$ ratios measured before and after the OL in two thin DC(T)s (Sp-1 and Sp-2), and the plastic zone sizes induced by the OL according to Irwin's estimate for *pl-σ*, $pz_{OL} = (1/\pi){\cdot}(K_{OL}/S_Y)^2$.

Fig. 16 shows FCG rates *da/dN* and $K_{op}/K_{max}$ ratios measured before and after an OL in two thick DC(T)s with $t = 30$ mm, Sp-1 and Sp-2.

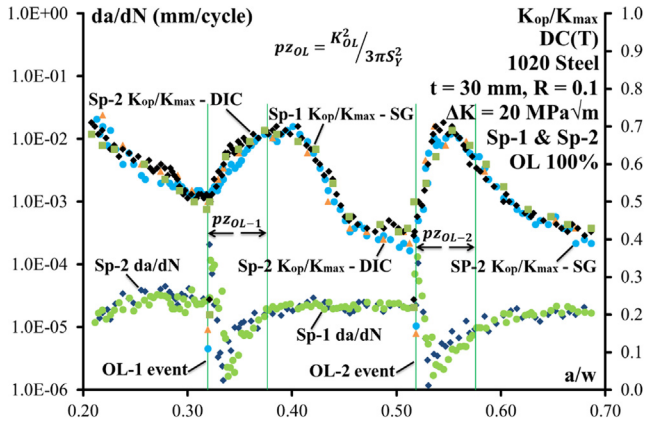


**Fig. 16.** FCG rates *da/dN* and crack-opening ratios $K_{op}/K_{max}$ continuously measured under quasi-constant amplitude loading conditions {$\Delta K = 20$ MPa√m, $R = 0.1$}, before and after two well-spaced OLs with $K_{OL} = 2{\cdot}K_{max}$, in two thick 1020 steel specimens with $t = 30$ mm.

They also show the size of the OL plastic zone according to Irwin's estimate for *pl-ε*; $pz_{OL} = (1/3\pi){\cdot}(K_{OL}/S_Y)^2$. In these specimens it is possible to apply two properly spaced OLs, since their *da/dN* rates stabilize more quickly after the OL when compared to the *pl-σ* tests. Notice that, like in Fig. 15, the OLs induce as well significant changes both in $K_{op}/K_{max}$ ratios and in *da/dN* FCG rates in these thick specimens, but they are not related.

Indeed, Figs. 15 and 16 show that the OLs induce significant delays in the subsequent FCG rates, but with *da/dN* and $K_{op}/K_{max}$ ratios out of phase. Moreover, the minimum *da/dN* rates during the delays do not correspond to the peak values of their $K_{op}/K_{max}$ ratios. Furthermore, after the maximum value of the $K_{op}/K_{max}$ ratio is reached, it remains almost constant as the FCG rate begins to recover as the crack moves away from the point where *da/dN* is minimal. Moreover, in the *pl-σ* tests the effects of the delay continues to affect the crack after it crosses $pz_{OL}$. Fleck found similar results [49], which he strangely attributed to "discontinuous closure", since they cannot be explained by Elber's PICC.

Similar OL tests under *pl-σ* and *pl-ε* are made in thin $t = 2$ mm and thick $t = 30$ mm 6351-T6 Al DC(T)s, keeping constant {$\Delta K = 15$ MPa√m, $R = 0.1$} loading conditions controlled by the automated system described above. The cracks grow until reaching $a \cong 6$ mm, when a single *100%* OL on $K_{max}$ with $K_{OL} = 33.33$ MPa√m is applied. Next, the almost constant {$\Delta K$, $R$} loadings are reapplied to continue propagating the crack. Figs. 17 and 18 show the FCG rates *da/*

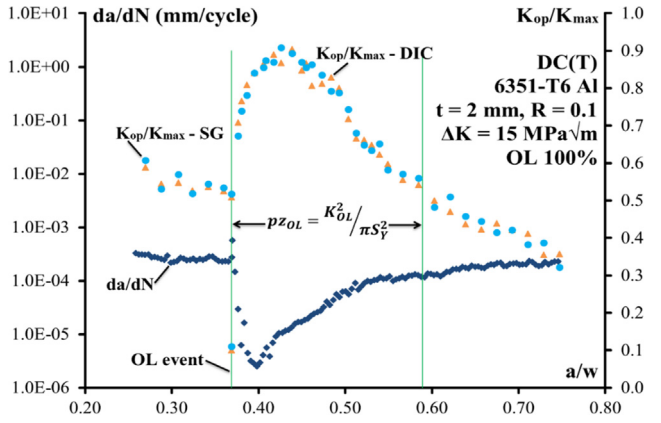


**Fig. 17.** FCG rates *da/dN* and crack-opening ratios $K_{op}/K_{max}$ continuously measured under quasi-constant amplitude loading conditions $\{\Delta K = 15$ MPa√m, $R = 0.1\}$, before and after a single OL with $K_{OL} = 2{\cdot}K_{max}$, in a thin 6351-T6 Al specimen with $t = 2$ mm.

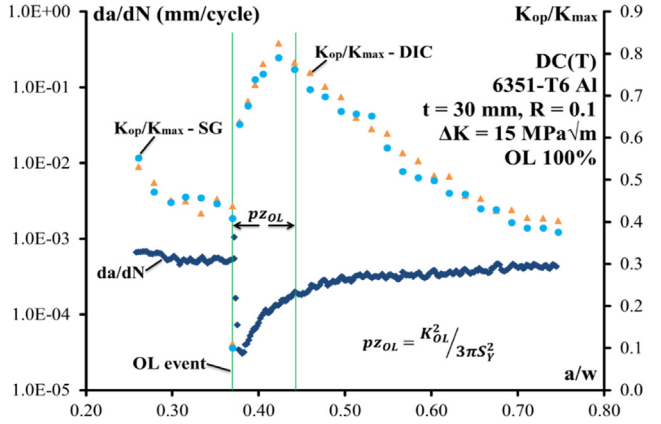


**Fig. 18.** FCG rates *da/dN* and crack-opening ratios $K_{op}/K_{max}$ continuously measured under quasi-constant amplitude loading conditions $\{\Delta K = 15$ MPa√m, $R = 0.1\}$, before and after a single OL with $K_{OL} = 2{\cdot}K_{max}$, in a thick 6351-T6 Al specimen with $t = 30$ mm.

*dN* and the $K_{op}/K_{max}$ ratios measured before and after the OL in the thin and thick DC(T)s, respectively. The figures also show $pz_{OL}$ sizes by Irwin's *pl-σ* and *pl-ε* estimates. Notice how the automated load control program considerably reduces the noise level of the measured FCG rates.

Notice as well that the minimum value of the FCG rates and the peak of the $K_{op}/K_{max}$ ratios are once again out of phase, as in the AISI 1020 steel tests, and that the OL effects are not completely eliminated when the crack reaches the border of $pz_{OL}$. Such results cannot be explained by $\Delta K_{eff}$ concepts either.

### 4.2. Stress/strain loops measured inside the reverse plastic zone ahead of the crack tip

Further tests are performed to measure the deformations inside the region with the reverse or cyclic plastic zone $pz_r$ near the crack tip, using the stereo microscope DIC system [48]. These tests are not trivial, because they require a large magnification to measure strains with a very severe gradient within the $pz_r$, whose size is estimated once again by Irwin as $pz_r = (1/\pi){\cdot}[\Delta K/(2{\cdot}S_Y)]^2$.

The parameters of the DIC analysis are a subset size of 41 × 41 pixels, a step size of 11 pixels and a strain window of 19 × 19. As mentioned before, the global strain field is measured simultaneously on the opposite face of the specimen with the conventional DIC system, and a strain-gage is bonded on the DC(T) back face. The first

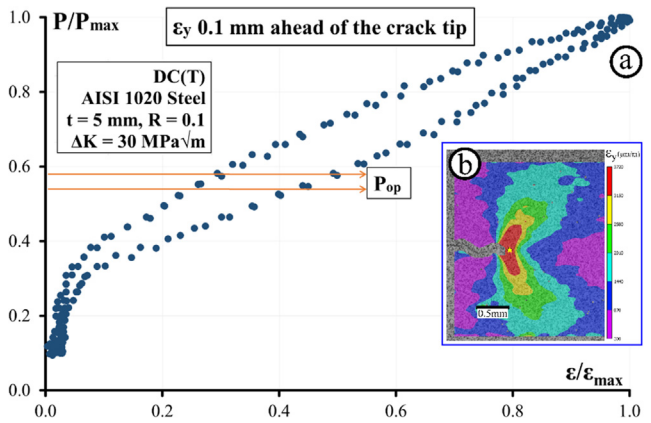


**Fig. 19.** Strain loop measured *0.1* mm ahead of the crack tip in the 1020 steel specimen.

measurements are made in a DC(T) 1020 steel specimen.

Assuming that Irwin's estimate for the reverse plastic zone $pz_r$ size is valid, then the quasi-constant amplitude loads $\{\Delta K = 30$ MPa√m, $R = 0.1\}$ are chosen to obtain a good resolution inside the estimated $pz_r = (1/\pi){\cdot}[\Delta K/(2S_Y)]^2 = (1/\pi){\cdot}[30/(2{\cdot}262)]^2 = 1.04$ mm. Since a DIC measurement can be made at every 17.6 μm (the DIC step), there are approximately *50* measurement points within the estimated $pz_r$. Moreover, since the thickness of the specimen is $t = 5$ mm and the monotonic plastic zone is $pz = (1/\pi){\cdot}(K_{max}/S_Y)^2 = 5.15$ mm, the crack is assumed to propagate under *pl-σ* conditions.

The loads are adjusted to maintain fixed $\{\Delta K, R\}$ conditions as the crack grows during the test, using once again the efficient home-made automated system. The crack propagates with an almost constant FCG rate $da/dN = 10^{-4}$ mm/cycle, until it is far from the influence of notch effects. At this point, $P_{op}$ is measured using the signals from the back face strain-gage and from the conventional DIC system, using the very same procedures described above.

Then, the DIC stereo microscope system is used to measure strain loops inside the $pz_r$ ahead of the crack tip. Two successive loading cycles are monitored taking *100* photos per cycle. Fig. 19b shows the vertical strain ($\varepsilon_y$) field measured at the maximum load in the direction of the load axis, perpendicular to the crack plane, and the point inside the $pz_r$ used to measure the strain loop. Fig. 19a shows a strain loop measured inside the $pz_r$, *0.1* mm ahead of the crack tip, as located by the star marker in Fig. 19b. Since this point width is less than 18 μm, it remains well within the $pz_r$. Moreover, since $P_{op} = 0.56{\cdot}P_{max}$, there is incremental strain activity ahead of the crack tip before it is fully open, both during the loading and during the unloading parts of the loading cycle. This fact clearly contradicts the Elberian hypothesis that assumes no activity ahead of the crack when $P < P_{op}$.

Following the same procedures, similar measurements are made with the stereo microscope DIC system in a 6351-T6 Al DC(T) specimen. The constant amplitude loads $\{\Delta K = 22.5$ MPa√m, $R = 0.1\}$ are once again chosen to obtain a good resolution inside the reverse plastic zone, which by Irwin's estimate is here $pz_r = (1/\pi){\cdot}(\Delta K/2S_Y)^2 = (1/\pi){\cdot}[22.5/(2{\cdot}170)]^2 = 1.39$ mm. Since a strain measurement is performed at every 17.6 μm (the DIC step), there are approximately *70* measurement points within the estimated $pz_r$. Since the thickness of the specimen is $t = 10$ mm, and the monotonic plastic zone (that is induced by $K_{max}$) is $pz = (1/\pi){\cdot}(K_{max}/S_Y)^2 = 6.88$ mm, it can be assumed that this crack is growing by fatigue under a dominant plane stress state (although perhaps not a pure one). After growing at an almost constant FCG rate $da/dN = 1.5{\cdot}10^{-3}$mm/cycle, until the crack tip is far from the region of influence of the notch effects, the opening load $P_{op}$ is carefully measured by all methods studied before, reaching a value $P_{op}/P_{max} = 0.54 \pm 0.02$. Then the strain loop is measured in front of the crack tip with the stereo microscope DIC system. Two loading cycles are

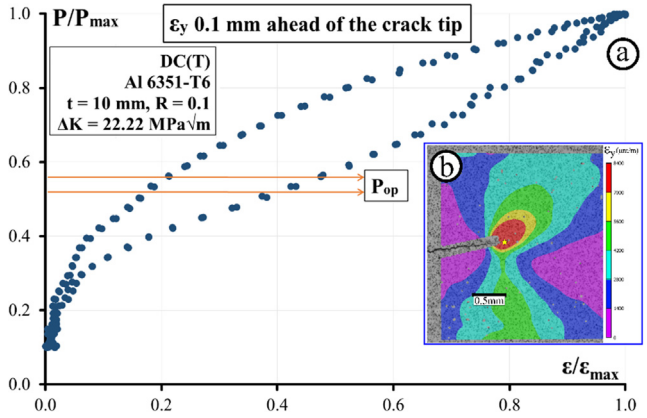


**Fig. 20.** Strain loop measured *0.1* mm ahead of the crack tip in the 6351-T6 Al specimen.

measured taking *100* photos per cycle. Fig. 20a shows a strain loop measured inside the $pz_r$, *0.1* mm ahead of the crack tip.

Like the strain loop measured inside the $pz_r$ of the steel specimen (depicted in Fig. 19a), the strain loop of the Al specimen, illustrated in Fig. 20a, shows that the strains steadily increase from $P_{min}$ at loads $P < P_{op}$. Like in the steel case, this loop is measured *0.1* mm ahead of the crack tip. Since the strain range $\Delta\varepsilon$ is the main cause or the driving force for fatigue damage according to well stablished $\varepsilon N$ concepts, Elber's hypothesis that assumes loads $P < P_{op}$ cannot contribute for fatigue damage is clearly contradicted by this experimental result. Finally, notice that the two lines associated with $P_{op}$ in Figs. 19 and 20 reflect the small dispersion of the various methods used to measure it.

## 5. Conclusions

Experimental data obtained in FCG tests under quasi-constant $\Delta K$ and $K_{max}$ load conditions, in DC(T) steel specimens and DC(T) and C(T) aluminum specimens, showed that the crack-opening ratio $K_{op}/K_{max}$ decreases as the crack length increases, while the FCG rate remains practically constant during the entire test. The decreasing behavior of the crack-opening ratio $K_{op}/K_{max}$ measured by four redundant methods, observed in thin and thick specimens with different geometries, showed no significant discrepancy in the testing results, confirming the reliability and repeatability of the data obtained in previous works. Since the $\Delta K_{eff}$ measured along those tests augmented significantly with the crack size, whereas the measured FCG rates $da/dN$ remained practically constant, it can be concluded that Elber's effective stress intensity factor range was not the actual FCG driving force for the analyzed tests.

In the overload tests both in aluminum and in steel specimens, the minimum value of $da/dN$ is considerably out of phase with respect to the maximum $K_{op}/K_{max}$ ratio (minimum $\Delta K_{eff}$). Moreover, in some tests (Figs. 16 and 18) the effects of the delay continue to affect the crack after it has crossed the overload plastic zone, which cannot be explained by the traditional theories of load sequence effects. This makes it impossible to correlate $\Delta K_{eff}$ with the $da/dN$ rate, so these results contradict Elber's hypothesis as well. Similar results are available in the literature, e.g. Fleck found similar data [49], which he however attributed to "discontinuous closure".

Figs. 19 and 20 show that there is significant strain variation in the EP loops measured within the $pz_r$ at loads $P < P_{op}$, at a point located just *0.1* mm ahead of the crack tip. This fact disputes Elber's hypothesis that assumes the region ahead of the crack tip is protected from any damage below $P_{op}$, or that the crack only suffers damage after being fully open. Moreover, it is notable that the shape of these EP loops within the $pz_r$ is very similar to the hysteresis loops of negative ratio $\varepsilon N$ tests, validating the crack propagation problem approach made by critical damage models [37–39]. Finally, it is worth emphasizing that since all the comprehensive data presented here clearly contradict $\Delta K_{eff}$ concepts, they certainly justify the word "challenging" used in this work title.

## Declaration of Competing Interest

The authors declare that they have no known competing financial interests or personal relationships that could have appeared to influence the work reported in this paper.

## Acknowledgement

Julián González would like to gratefully acknowledge the support of FAPERJ – Fundação de Amparo à Pesquisa do Estado do Rio de Janeiro, Process number 201.699/2017.

## References

[1] Paris PC, Gomez MP, Anderson WEP. A rational analytic theory of fatigue. Trend Eng 1961;13:9–14.
[2] Paris PC, Erdogan F. A critical analysis of crack propagation laws. J Basic Eng 1963;85:528–34. https://doi.org/10.1115/1.3656900.
[3] Castro JTP, Meggiolaro MA. Fatigue design techniques, vol. 3: crack propagation, temperature and statistical effects. CreateSpace 2016.
[4] Elber W. Fatigue crack closure under cyclic tension. Eng Fract Mech 1970;2:37–45. https://doi.org/10.1016/0013-7944(70)90028-7.
[5] Elber W. The significance of fatigue crack closure. Damage Tolerance in Aircraft Structures, ASTM STP 486; 1971: 230–42. https://doi.org/10.1520/STP26680S.
[6] von Euw EFG, Hertzberg RW, Roberts R. Delay effects in fatigue crack propagation. ASTM STP 513; 1972: 230–59. https://doi.org/10.1520/STP34123S.
[7] McEvily AJ. Current aspects of fatigue. Metal Sci 1977;11:274–84. https://doi.org/10.1179/msc.1977.11.8-9.274.
[8] Schijve J. Four lectures on fatigue crack growth. Eng Fract Mech 1979;11:176–221. https://doi.org/10.1016/0013-7944(79)90038-9.
[9] Newman JC. A crack-closure model for predicting fatigue crack growth under aircraft spectrum loading. Methods and Models for Predicting Fatigue Crack Growth under Random Loading, ASTM STP 748; 1981: 53–84. https://doi.org/10.1520/STP28334S.
[10] de Koning AU, Liefting G. Analysis of crack-opening behavior by application of a discretized strip yield model. Mechanics of Fatigue Crack Closure, ASTM STP 982; 1988: 437–58. https://doi.org/10.1520/STP27224S.
[11] Newman JC. An evaluation of the plasticity-induced crack-closure concept and measurement methods. NASA/TN-1998-208430, Langley Research Center; 1998.
[12] Beretta S, Carboni M. A strip-yield algorithm for the analysis of closure evaluation near the crack tip. Eng Fract Mech 2005;72:1222–37. https://doi.org/10.1016/j.engfracmech.2004.10.003.
[13] Yamada Y, Newman JC. Crack closure under high load-ratio conditions for Inconel-718 near threshold behavior. Eng Fract Mech 2009;76:209–20. https://doi.org/10.1016/j.engfracmech.2008.09.009.
[14] Kemp PMJ. Fatigue crack closure – a review. TR90046. UK: Royal Aerospace Establishment; 1990.
[15] Skorupa M. Load interaction effects during fatigue crack growth under variable amplitude loading – a literature review – part I: empirical trends. Fatigue Fract Eng Mater Struct 1998;21:987–1006. https://doi.org/10.1046/j.1460-2695.1998.00083.x.
[16] Skorupa M. Load interaction effects during fatigue crack Growth under variable amplitude loading – a literature review – part II: qualitative interpretation. Fatigue Fract Eng Mater Struct 1999;22:905–26. https://doi.org/10.1046/j.1460-2695.1999.00158.x.
[17] Pippan R, Hohenwarter A. Fatigue crack closure: a review of the physical phenomena. Fatigue Fract Eng Mater Struct 2017;40:471–95. https://doi.org/10.1111/ffe.12578.
[18] Castro JTP, Meggiolaro MA, Miranda ACO. Singular and non-singular approaches for predicting fatigue crack growth behavior. Int J Fatigue 2005;27:1366–88. https://doi.org/10.1016/j.ijfatigue.2005.07.018.
[19] Chen DL, Weiss B, Stickler R. The effective fatigue threshold: significance of the loading cycle below the crack-opening load. Int J Fatigue 1994;16:485–91. https://doi.org/10.1016/0142-1123(94)90199-6.
[20] Vasudevan AK, Sadananda K, Holtz RL. Analysis of vacuum fatigue crack growth results and its implications. Int J Fatigue 2005;27:1519–29. https://doi.org/10.1016/j.ijfatigue.2005.07.026.
[21] Vasudevan AK, Sadananda K, Holtz RL. Unified approach to fatigue damage evaluation. NRL Rev 2003:51–7.
[22] Vasudevan AK, Sadananda K, Louat N. Reconsideration of fatigue crack closure. Scripta Metall Mater 1992;27:1663–78. https://doi.org/10.1016/0956-716X(92)90164-A.
[23] Vasudevan AK, Sadananda K, Louat N. A review of crack closure, fatigue crack threshold and related phenomena. Mater Sci Eng 1994;188A:1–22. https://doi.org/10.1016/0921-5093(94)90351-4.
[24] Sadananda K, Vasudevan AK. Crack tip driving forces and crack growth

representation under fatigue. Int J Fatigue 2004;26:39–47. https://doi.org/10.1016/S0142-1123(03)00105-1.
[25] Kujawski D. A new $(\Delta K^{+}K_{max})^{0.5}$ driving force parameter for crack growth in aluminum alloys. Int J Fatigue 2001;23:733–40. https://doi.org/10.1016/S0142-1123(01)00023-8.
[26] Kujawski D. $\Delta K_{eff}$ parameter under re-examination. Int J Fatigue 2003;25:793–800. https://doi.org/10.1016/S0142-1123(03)00129-4.
[27] Dinda S, Kujawski D. Correlation and prediction of fatigue crack growth for different R-ratios using $K_{max}$ and $\Delta K^{+}$ parameters. Eng Fract Mech 2004;71:1779–90. https://doi.org/10.1016/j.engfracmech.2003.06.001.
[28] Sadananda K, Vasudevan AK. Fatigue crack growth mechanisms in steels. Int J Fatigue 2003;25:899–914. https://doi.org/10.1016/S0142-1123(03)00128-2.
[29] Castro JTP. Some critical remarks on the use of potential drop and compliance systems to measure crack growth in fatigue experiments. J Braz Soc Mech Sci Eng 1985;7:291–314.
[30] Toda H, Sinclair I, Buffière JY, Maire E, Connolley T, Joyce M, et al. Assessment of the fatigue crack closure phenomenon in damage-tolerant aluminium alloy by in-situ high-resolution synchrotron X-ray microtomography. Philos Mag 2003;83:2429–48. https://doi.org/10.1080/14786430310001157 54.
[31] Withers PJ, Preuss M. Fatigue and damage in structural materials studied by x-ray tomography. Annu Rev Mater Res 2012;42:81–103. https://doi.org/10.1146/annurev-matsci-070511-155111.
[32] Schijve J. Fatigue of structures and materials. Kluwer; 2001.
[33] Ruckert COFT, Tarpani JR, Milan MT, Bose WW, Spinelli D. Evaluating Berkovitz's K-parametrization method to predict fatigue loads in failure investigations. Proceedings SAE Fatigue 2004, paper 2004-01-2211. https://doi.org/10.1361/105994906X150759.
[34] NASGRO Fracture Mechanics and Fatigue Crack Growth Analysis Software Reference Manual, Version 4.02, NASA 2002.
[35] Newman JC. A crack-opening stress equation for fatigue crack growth. Int J Fract 1984;24:R131–5. https://doi.org/10.1007/BF00020751.
[36] Newman JC, Crews JH, Bigelow CA, Dawicke DS. Variations of a global constraint factor in cracked bodies under tension and bending loads. ASTM STP 1244; 1995: 21–42. https://doi.org/10.1520/STP14629S.
[37] Ferreira SE, Castro JTP, Meggiolaro MA. Using the strip-yield mechanics to model fatigue crack growth by damage accumulation ahead of the crack tip. Int J Fatigue 2017;103:557–75. https://doi.org/10.1016/j.ijfatigue.2017.06.039.
[38] Ferreira SE, Castro JTP, Meggiolaro MA. Fatigue crack growth predictions based on damage accumulation ahead of the crack tip calculated by strip-yield procedures. Int J Fatigue 2018;115:89–106. https://doi.org/10.1016/j.ijfatigue.2018.03.001.
[39] Ferreira SE, Castro JTP, Meggiolaro MA, Miranda ACO. Crack closure effects on fatigue damage ahead of crack tips. Int J Fatigue 2019;125:187–98. https://doi.org/10.1016/j.ijfatigue.2019.03.039.
[40] Paris PC; Hermann L. Twenty years of reflections on questions involving fatigue crack growth, part II: some observations of fatigue crack closure. Fatigue Thresholds 1:11-33, EMAS 1982.
[41] González JAO, Castro JTP, Gonzáles GLG, Meggiolaro MA, Freire JLF. Verification of the $\Delta K_{eff}$ hypothesis along the fatigue crack path in thin and thick Al specimens. Frattura ed Integrità Strutturale 2019;49:26–35. https://doi.org/10.3221/IGF-ESIS.49.03.
[42] González JAO, Castro JTP, Gonzáles GLG, Meggiolaro MA, Freire JLF. On DIC measurements of $\Delta K_{eff}$ to verify if it is the FCG driving force. Frattura ed Integrità Strutturale 2017;41:227–35. https://doi.org/10.3221/IGF-ESIS.41.31.
[43] Castro JTP, Meggiolaro MA, González JAO. Can $\Delta K_{eff}$ be assumed as the driving force for fatigue crack growth? Frattura ed Integrità Strutturale 2015;33:97–104. https://doi.org/10.3221/IGF-ESIS.33.13.
[44] Corbani S, Castro JTP, Miranda ACO, Martha LF, Carter BJ, Ingraffea AR. Crack shape evolution under bending-induced partial closure. Eng Fract Mech 2018;188:493–508. https://doi.org/10.1016/j.engfracmech.2017.10.002.
[45] Miranda ACO, Meggiolaro MA, Castro JTP, Martha LF. Crack retardation equations for the propagation of branched fatigue cracks. Int J Fatigue 2005;27:1398–407. https://doi.org/10.1016/j.ijfatigue.2005.07.016.
[46] Gonzáles GLG, González JAO, Castro JTP, Freire JLF. A J-integral approach using digital image correlation for evaluating stress intensity factors in fatigue cracks with closure effects. Theor Appl Fract Mech 2017;90:14–21. https://doi.org/10.1016/j.tafmec.2017.02.008.
[47] Sutton MA, Orteu JJ, Schreier HW. Image correlation for shape, motion and deformation measurements. Springer; 2009.
[48] Gonzáles GLG, González JAO, Castro JTP, Freire JLF. Using DIC techniques to measure strain ranges inside the cyclic plastic zone ahead of a fatigue crack tip. Frattura ed Integrità Strutturale 2019;13:74–81. https://doi.org/10.3221/IGF-ESIS.49.08.
[49] Fleck NA. Influence of stress state on crack growth retardation. Basic Questions in Fatigue. ASTM STP 1988;924(1):157–83. https://doi.org/10.1520/STP23215S.